Investigation of Antennas Integrated Into Disposable Unmanned Aerial Vehicles

Sung Yun Jun, Anshuman Shastri, Benito Sanz-Izquierdo, David Bird, and Alan McClelland

***Abstract*—The integration of antennas into disposable paper drones using inkjet printing technology is presented. These drones or unmanned aerial vehicles (UAVs) are developed using origami folding structures. Two vertical monopole antennas based on the same design concept are proposed and their performance assessed for two different conditions. The conditions relate to the placement of the other electronic components and circuits on the origami drones as reported in the literature. The first is when the electromechanical components and corresponding metallic layers are located in the wings. In this case, the effect of the possible location of the antenna as well as the deformation of the wings on S_{11} is discussed. The second is a more general case scenario which includes when the components and motors are placed at the tail and lower part of the body of the drone. The antenna elements are directly printed onto a photo paper substrate using silver nanoparticle conductive ink. Subsequently, the substrate is folded to create a paper drone. Low-cost desktop inkjet printing equipment is used to deposit the metallic tracks of the antenna. The designs target the current frequency bands employed in the control and wireless communication of commercial drones (2.4 GHz and 5 GHz bands). The purpose of this work is to investigate potential antenna scenarios for disposable drones which may one day be fully fabricated using inkjet printing technology. All antenna designs and studies have been simulated using CST Microwave Studio and compared well with experimental results.**

***Index Terms*—Antennas, inkjet printing, origami, unmanned aerial vehicles (UAVs).**

I. Introduction

UNMANNED aerial vehicles (UAVs), otherwise known as drones, have become very popular in fields such as food and agricultural sector, industry electronics, intelligent transportation systems and safety and security [1]–[8]. One critical factor in UAVs is the wireless communication system where coverage and capacity is crucial [7], [8] for the reliable operation of a drone. For large coverage capabilities, drones sometimes require omnidirectional antennas where signal levels are mostly equal in all directions. Antennas are selected, designed and developed to meet these specifications in both commercial and defense applications. The antennas can be located either inside or outside of the drone structure. One or more elements are typically used to cover technologies such as Bluetooth, GPS, WIFI and LTE [9]. In [13], for example, a conformal antenna is installed on the shell structure of a drone made of carbon fiber materials. In [14], a dipole structure with a radiator, feeding strips and a reflector, is arranged so that it offers horizontal polarization. A planar segmented loop patch antenna that offers omnidirectional and quasi-omnidirectional radiation patterns and operates over the wide bandwidth, is presented in [15]. A lightweight blade antenna is proposed and discussed in [16]. In [17], a triple band patch antenna is fabricated on a Duriod substrate and then connected to the other components inside the drone. In all these cases, the antenna and drone structure are fabricated using conventional manufacturing methods.

With the increasing use of additive manufacturing (AM) in the aerospace sector, it makes sense for UAVs [18] and corresponding antennas to be fabricated using AM techniques. Inkjet printing is a potential AM technology to apply. It allows the easy fabrication and prototyping of antennas on various substrates. The inkjet printing of antennas has been proposed for a variety of applications. For example, a flexible inkjet-printed broadband UHF Radio Frequency Identification (RFID) on liquid crystal polymer (LCP) substrate is developed for sensing applications in [19]. A multilayer millimeter-wave yagi-uda antenna and proximity-fed patch arrays on flexible substrates using purely additive inkjet printing technology is proposed in [20], [21]. A compact inkjet-printed ultrawideband antenna on a Kapton polyimide substrate is used for flexible and wearable electronics in [22]. A monopole antenna on a paper substrate for wireless communication is discussed in [23], and a phased-array antenna implemented by inkjet-printed barium strontium titanate (BST) thick-films in [24].

Disposable drones are currently attracting significant research interest [25], [26]. These drones should be made of inexpensive and degradable materials such as paper or cellulose based materials. Components such as inertial sensors and elevons can be integrated into such drones using AM techniques [26]. Furthermore, actuators and potential motors have been developed for this application [27].

This paper presents a study on the integration of antennas into origami disposable drones. Two antennas based on a similar

Manuscript received December 18, 2017; revised May 12, 2018 and September 6, 2018; accepted October 22, 2018. Date of publication November 29, 2018; date of current version January 15, 2019. This work was supported in part by the UK EPSRC High Value Manufacturing Fellowship (REF: EP/L017121/1), in part by the CHIST ERA under EPSRC grant (EP/P015840/1) and in part by the Royal Academy of Engineering Industrial Secondment scheme (REF: ISS1617/48). The review of this paper was coordinated by Dr. Y. Gao. *(Corresponding author: Benito Sanz-Izquierdo.)*

S. Y. Jun, A. Shastri, and B. Sanz-Izquierdo are with the School of Engineering and Digital Arts, University of Kent, Canterbury CT2 7NT, U.K. (e-mail: sj329@kent.ac.uk; as2256@kent.ac.uk; b.sanz@kent.ac.uk).

D. Bird and A. McClelland are with the Centre for Process Innovation (CPI), Durham TS21 3FE, U.K. (e-mail: david.bird@uk-cpi.com; Alan.McClelland@uk-cpi.com).

Color versions of one or more of the figures in this paper are available online at http://ieeexplore.ieee.org.

Digital Object Identifier 10.1109/TVT.2018.2882791

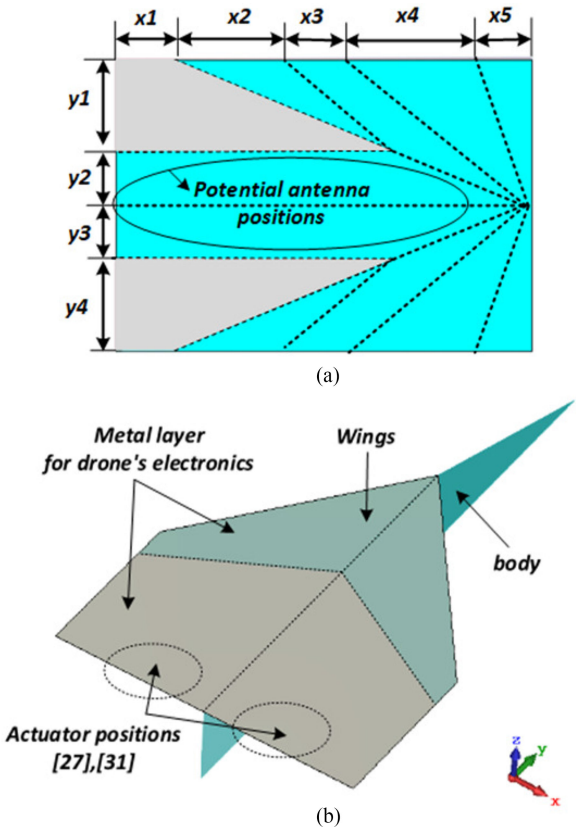

Fig. 1. Realized paper drone geometry of (a) the unfolded planar photo paper sheet and (b) perspective view of paper drone.

TABLE I
UNFOLDED PLANAR SHEET [MM]

x1	*x2*	*x3*	*x4*	*x5*	*y1*	*y2*	*y3*	*y4*
40	60	50	90	50	70	35	35	70

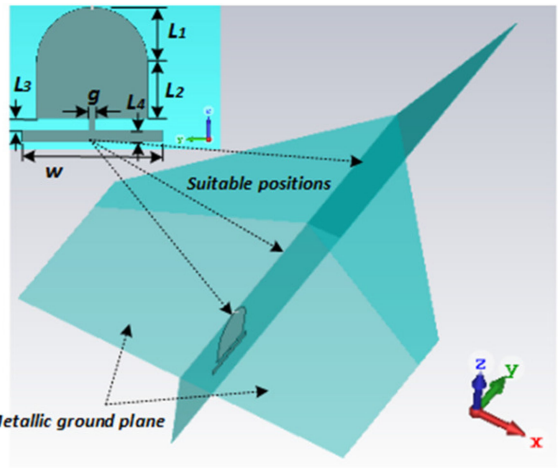

Fig. 2. Antenna dimensions and potential positions on an origami drone with a large metallic ground plane covering the top of the wings.

design concept are assessed for two conditions. The first is when all electronic components and the ground plane are located on the wings. The second is a when the electronic components are at the bottom of the drone and the antenna needs to be fed from bottom up. The latter uses a coplanar waveguide fed line which is used for the analysis of the deposited metallic layers. Inexpensive fabrication equipment, and silver nanoparticle ink has been employed for the fabrication of the antennas. The antennas are designed to cover the 2.4 GHz and 5 GHz bands currently specified in the communication of drones [17], [28]. This includes transmission of a large amount of data for potential video recording applications at 5.8 GHz. This is the first time that antennas are studied for integration with disposable origami drones, particularly involving inkjet printing and realistic scenarios with vertically polarized antennas. The antennas have been designed taking into account the limitations of inkjet printing technologies such as the potential damage and cracks of conducting tracks when folding the printing layers. Thus, any folding of the antennas has been avoided.

This paper is organized as follows. Section II describes the foldable paper drone and proposes a suitable antenna structure for a first case scenario. Section III presents an optimized antenna design for a more general case and discusses printing issues. A conclusion and final discussion are included in Section IV. All simulations in this paper have been carried out using the finite integration technique (FIT) included in CST Microwave Studio [29].

II. ANTENNA DESIGN AND ANALYSIS

A. Antenna Design and Integration With a Drone's Electronics

One of the simplest forms of disposable drone can be developed using origami techniques where a piece of paper, as illustrated in Fig. 1(a) can be folded to produce the drone in Fig. 1(b). The dash lines in Fig. 1(a) indicate where the drone is folded and the corresponding dimensions are given in Table I. The paper is an A4 paper sheet of 210 mm $\times$ 290 mm. The dielectric constant and thickness of the paper were set according the manufacturer's datasheet at 3 and 0.18 mm respectively. This type of paper airplane is able to provide stable gliding flight even when loaded with additional avionic control systems [25]. These control systems can consist of small elevon tabs to steer the wings. Additional components for the propelling such as actuators could also be added [30]. As described in [27], [31], a large part of the electronics, subsystems and components for UAVs is positioned on the body and wings of the paper airplane. In Fig. 1(b), the top of the wings are made conductive to simulate this condition.

A vertically polarized monopole is ideal for this application as illustrated in Fig. 2. In this figure, the wings have been made transparent to show the antenna. The antenna can be connected to the other RF components in the wings through a 50 Ω transmission line or a dedicated matching network. The target frequencies are 2.4 GHz, 5.2 GHz and 5.8 GHz wireless bands [17], [28], which means a multiband antenna is

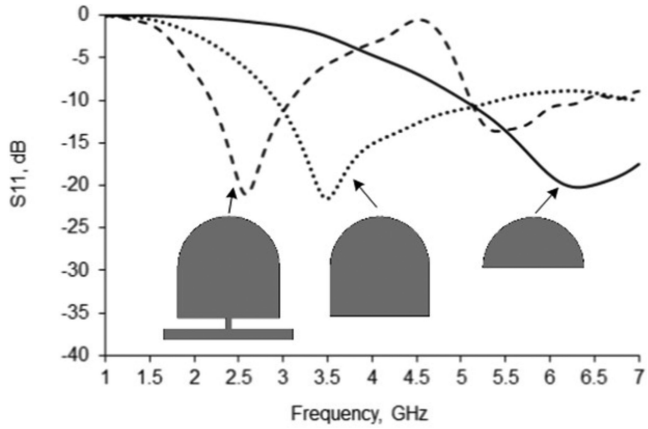

Fig. 3. Design process of the antenna with corresponding S_{11}.

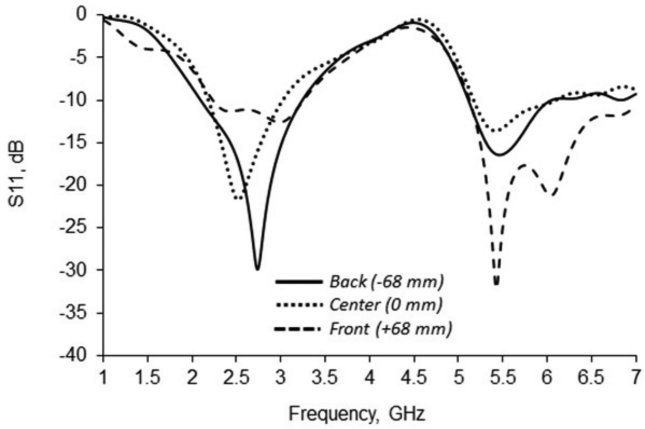

Fig. 4. Effect of antenna location on S_{11}.

TABLE II
DIMENSION OF THE INITIAL ANTENNA WITH LARGE GROUND PLANE [mm]

L_1	L_2	L_3	L_4	g	w
9.5	9.5	2	2	1	24

desirable. The aimed frequency bands are 2.4 GHz to 2.5 GHz and 5.15 GHz to 5.9 GHz. The first antenna design capable of achieving these specifications (Fig. 2) is based on a modified semicircle with a rectangular shape and a resonant element added at the top. The semicircle (L_1) provides matching for the large bandwidth necessary at the higher band, and the additional T-shape element with the matching gap L_3 are used to provide the lower band while not significantly increasing the size of the antenna.

A guideline on the design process is illustrated in Fig. 3. This includes graphs showing the corresponding reflection coefficient (S_{11}). The final dimensions are shown in Table II. The -10 dB S_{11} bandwidths are from 1.9 GHz to 2.7 GHz and from about 5.1 GHz to 5.9 GHz. There is a linear relationship between the operating wavelengths and the main parameters w and $L2$. This can be expressed by the equations:

$$\lambda 1 = 1.8\mathrm{w} \quad + 0.0724 \tag{1}$$

$$\lambda 2 = 4.7L2 \quad + 0.0048 \tag{2}$$

where $\lambda 1$ and $\lambda 2$ are the lower and higher wavelength band respectively. The unit in these equations is meters. The R-squared are 96% and 99% at the lower and higher wavelength band respectively. Further theoretical background for an antenna with semi-circular radiator can be found in [32].

Fig. 4 shows the S_{11} when the radiating element is placed at 3 different positions (Fig. 2): centered, at the back and at the front of the metallic ground plane. In all conditions, the antenna covers the intended frequency bands with S_{11} less than -10 dB. The depth of S_{11} and the bandwidth varies slightly for the three locations. The variations are due to the different coupling and impedances created between the radiating element and the area of the ground plane in close proximity to it.

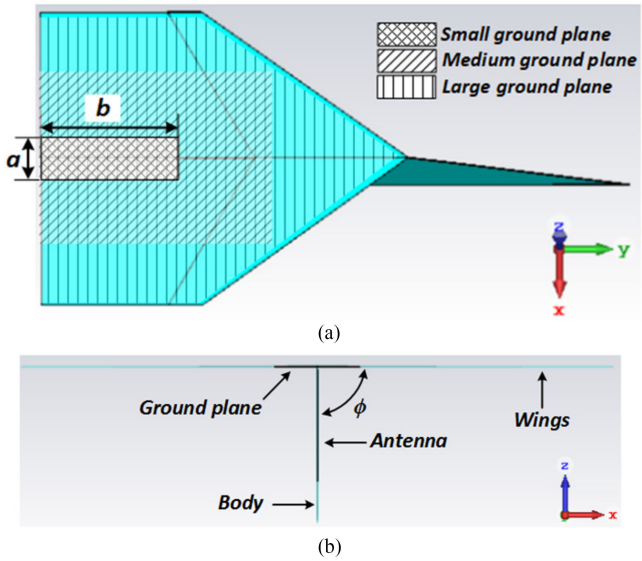

Fig. 5. Antenna optimized for a small ground plane. (a) Top view. (b) Back view.

TABLE III
DIMENSION OF THE ANTENNA OPTIMIZED FOR SMALL GROUND PLANE [mm]

L_1	L_2	L_3	L_4	g	w	a	b
8.5	12	2	3.5	1	24	20	60

B. Simplified Design and Effect of Smaller Ground

In order to simplify the fabrication process and to analyze the case where the electronics components occupy a smaller area on the wing of the plane, the size of the metallic ground plane was decreased as shown in Fig. 5. The antenna is the same as in Fig. 2 but the the radiating element has been optimized for the smaller ground (20 mm $\times$ 50 mm). The new dimensions are given in Table III. L_1, L_2 and L_4 are the parameters optimized.

In most vehicles as well as large drones, the size of the ground plane is very large compared with the operating wavelength. In our case, the size of the ground plane is relatively

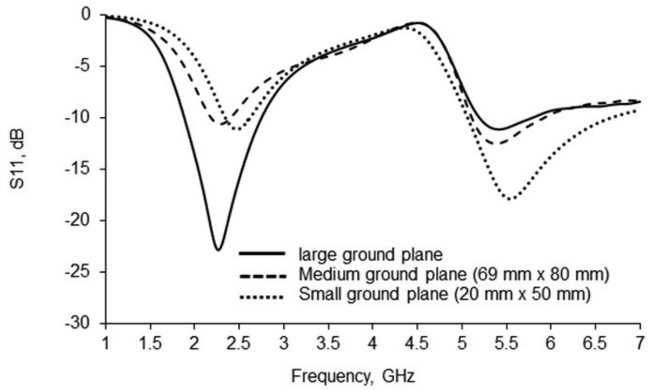

Fig. 6. S_{11} of the antenna with dimensions as in Table III for different ground plane dimensions. Large ground plane corresponds to ground plane as in Fig. 1.

small and its dimensions can change the impedance match of the antenna. Fig. 6 shows the S_{11} of the antenna with dimensions in Table III for different sizes of the ground plane (Fig. 5(a)). The antenna optimized for the small ground plane is able to cover the lower and higher frequency bands with S_{11} less than -10 dB. However, as the size of the ground plane is increased, the S_{11} at the higher frequency increases to a point where the intended band is not fully covered. The gain increases when the size of the ground plane increases. For this reasons, two antenna dimensions are provided here. One for the small (Table III) and another for the large (Table II) ground plane.

The surface current distributions of the antenna, with small ground, at three resonant frequencies (2.4 GHz, 5.2 GHz and 5.8 GHz) are depicted in Fig. 7. At 2.4 GHz, the current flows around the overall antenna (the modified semicircle with a rectangular shape and the top resonant element) and the ground plane.

By contrast, the surface current distribution concentrates around the feed of the radiating element and the bottom of the resonant element at 5.2 GHz and 5.8 GHz, as shown in Fig. 7(b) and (c) respectively.

C. Effect of Wing Deformation on Antenna Performance

The wings of a drone are typically exposed to tensions and deformations during flight operation. This can be significant in the case of paper drones. In addition, paper drones are expected to be folded by hand and therefore the wings may not be at exactly 90° from the base after the plane has been folded. For this reason, a study of the effect of changes in the angle ϕ (Fig. 5(b)) on S_{11} and the radiation patterns have been carried out. Fig. 8 presents the S_{11} of the antenna for values of ϕ of 60°, 90° and 120°. ϕ varies the angle of the metallic ground plane to the radiating element of the antenna. Therefore, the matching of the antenna changes for different angles of the folding of the wings. The frequency of operation and the input matching decrease when ϕ is decreased. The -10 dB bandwidth narrows at lower band but becomes wider at higher band. Further analysis indicates that the antenna is able to cover the 2.4 GHz, 5.2 GHz and 5.8 GHz bands ($S_{11} < -10$ dB) for angles of ϕ between 77° and 103°. The *xz* plane was used to analyze the effect on the radiation pattern at 2.4 GHz and 5.2 GHz as shown in Fig. 9. All radiation patterns are very similar for the folding angles studied.

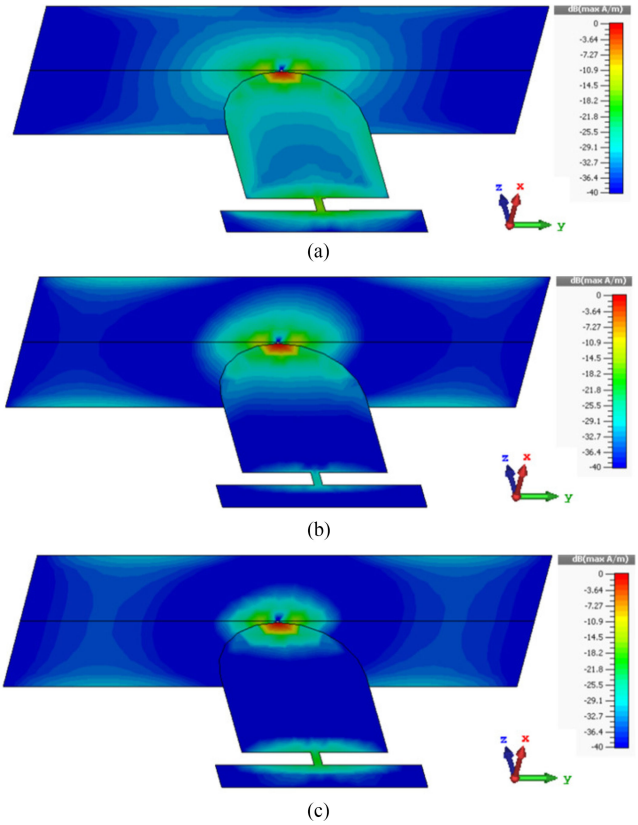

Fig. 7. Surface currents for the antenna design in Fig. 3. (a) 2.4 GHz. (b) 5.2 GHz. (c) 5.8 GHz.

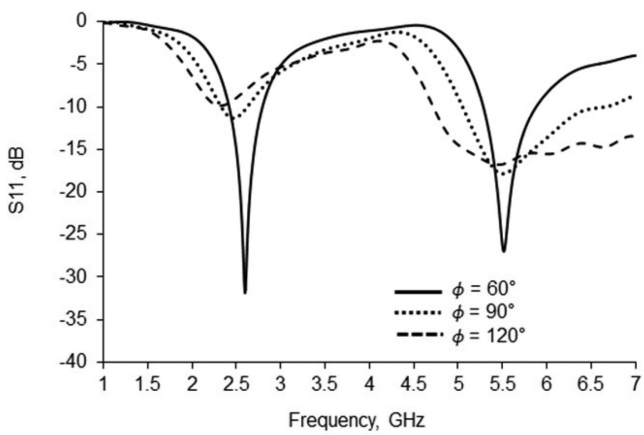

Fig. 8. Effect of changes in angle ϕ on S_{11}.

D. Fabrication and Measurement

The 3D model with the antenna elements and the ground plane were converted into a 2D model and positioned on a

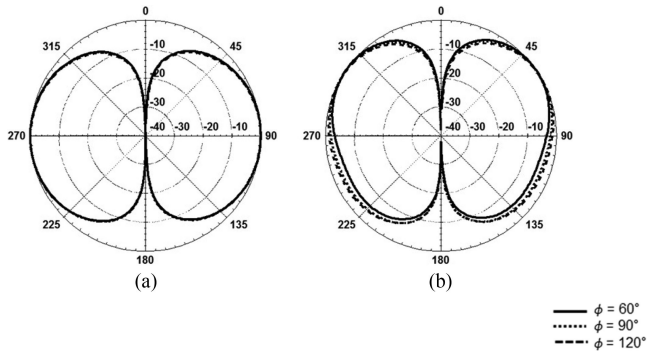

Fig. 9. Effect of changes in angle ϕ on the xz plane of the radiation pattern (a) at 2.4 GHz and (b) at 5.2 GHz.

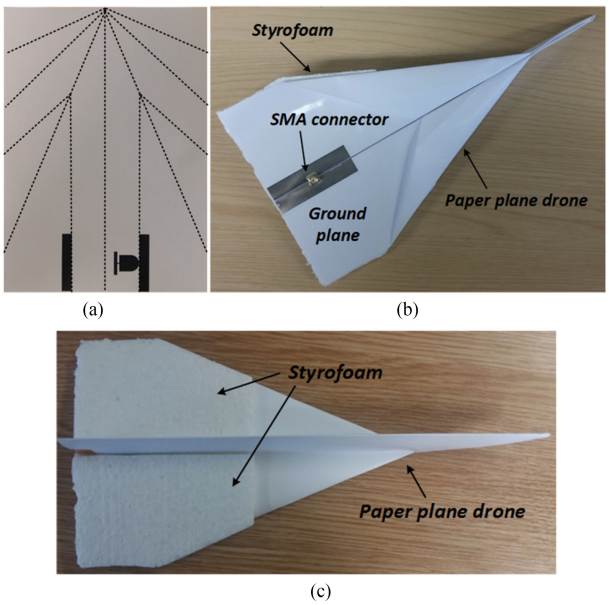

Fig. 10. Photograph of (a) printed planar photo paper sheet, (b) the origami paper drone, and (c) front view of the drone.

planar substrate as shown in Fig. 10(a). The 2D model, with the antenna and the ground plane, was exported to ViewMate from CST Microwave Studio with Gerber file (single layer). It was then converted to a PDF file.

The antenna and ground plane were printed directly onto the AgIC_CP01A4 photo paper with AgIC-AN01 Silver Nano Ink [33]. The Silver Nano Ink on the special coated paper provides conductivity of about 0.2 Ω/sq [33]. An MFC-J5910DW desktop inkjet printer from Brother Industries Ltd, USA was used. Conductive ink cartridges provided by AgIc Inc. replaced the normal colour ink cartridges in the printer. Conductivity emerges after a few seconds when the patterns were printed on the paper sheet. The antenna is expected to be functional as long as the printed conductive layers are not damaged and there is continuity throughout the metallic patterns that make the resonant element. Mechanical and thermal stability of the printed layers were provided by the manufacturer of the ink. In terms of thermal stability, heat resistance is allowed up to 30 minutes at 100 °C. The mechanical stability achieved in cross cut tests

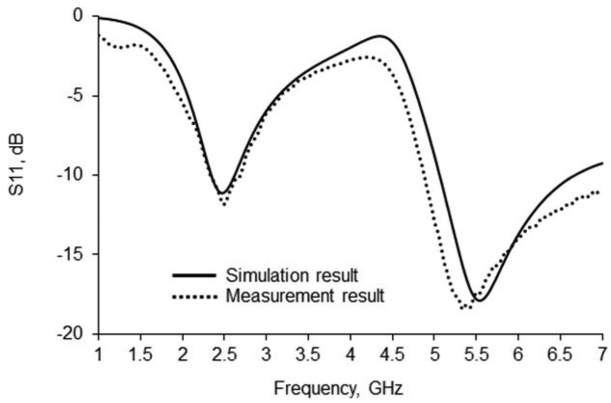

Fig. 11. Reflection coefficient (S_{11}) of the optimized antenna with a small ground plane.

(ISO 2409) is between 0 to 1 (0 is highest and 5 is lowest). A photograph of the fabricated paper plane drone is shown in Fig. 10. A 50 ohm SMA connector was attached to the center of the ground plane using silver epoxy conductive glue.

Similarly to the simulation model, the antenna was vertically positioned on the drone. In order to keep ϕ at 90° during the measurement, two rectangular blocks made of Styrofoam ($\varepsilon_r \approx 1$) were attached at the back sides of the wings.

Fig. 11 shows the reflection coefficient (S_{11}) of the antenna with a small ground plane. The measured S_{11} was obtained using an Anritsu 37397C vector network analyzer. The measured S_{11} is about -11 dB, -17 dB and -15 dB at 2.4 GHz, 5.2 GHz and 5.8 GHz respectively with bandwidths (<-10 dB) of 400 MHz at the lower band and 2200 MHz at the higher bands. The small difference between the simulated and the measured results is probably due to fabrication and measurement related errors. These include the non-uniform deposited silver conductive ink of the printed antenna and ground plane, the bending of the thick photo paper substrate, and the SMA connector. An analysis of the printed conductive layers is included in Section III.

The measured radiation patterns at 2.4 GHz, 5.2 GHz and 5.8 GHz are shown in Fig. 12. The patterns are dipole-like and mostly omnidirectional at the 2.4 GHz band. At the 5 GHz bands, the patterns become more monopole-like with mostly omnidirectional behavior in the xy plane but with a downward direction in the yz plane. The measured gains at 2.4 GHz, 5.2 GHz and 5.8 GHz are 1.7 dB, 2.2 dB and 2.5 dB respectively. The measured gains are between 0.2 dB (2.4 GHz) to 0.6 dB (5.8 GHz) higher than the simulations due to the effect of connectors and cables. The downward direction at the higher frequency band may be useful in the cases where the controller of the drone is positioned below the antenna. However, this could reduce the range of the control or potential data transmission when flying at positions where the controller is at the same height or higher than the drone.

As indicated earlier, this first antenna configuration is ideal for situations when most of the electronic components are located on the wing section of the drone which limits the possibility for improving the radiation patterns at the higher frequency band.

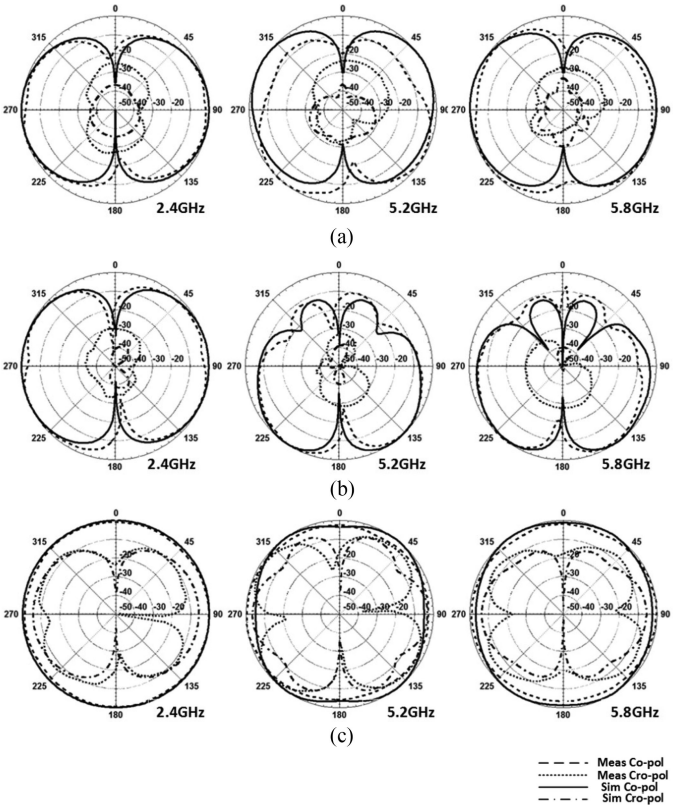

Fig. 12. Radiation patterns of the antenna on small ground plane (a) at *xz* plane, (b) at *yz* plane, and (c) at *xy* plane.

III. Second Antenna Solution and Analysis of the Printed Conductive Layers

A. Antenna Design

This section proposes a vertically polarized antenna where the antenna connection is at the base of the paper drone. This antenna is also used to assess the metallic ink layers deposited in the fabrication process. Fig. 13 shows the antenna design and its placement within the drone. The antenna is small enough to be hidden inside the vertical section of the plane and isolated from the external environment that could damage the inkjet printed metallic tracks [30]. The radiator consists of a semicircle with an additional rectangular resonant element separated by a gap and connected by a small rectangular track. The radiating component is fed by a coplanar waveguide transmission line. The dielectric constant, tangent loss and thickness of the substrate are the same as the earlier design. The desired resonant frequency and bandwidth were obtained by adjusting the size and the length of the radiation elements and the gap between feed line and the ground plane surfaces.

The dimensions of the ground plane were crucial for the optimization for the radiation pattern. The final dimensions of the antenna are given in Table IV.

The surface current distribution at 2.4 GHz, 5.2 GHz and 5.8 GHz are shown in Fig. 14. At 2.4 GHz, the surface current is strong and evenly distributed through the feed line, the semicircle and the top resonant element while it is small in the middle sections of the ground plane. At 5.2 GHz, the currents are spread more uniformly in the ground plane and towards the edges of the radiator. At 5.8 GHz, the currents tend to concentrate more towards the center of the antenna and the gap between the radiator and the ground plane.

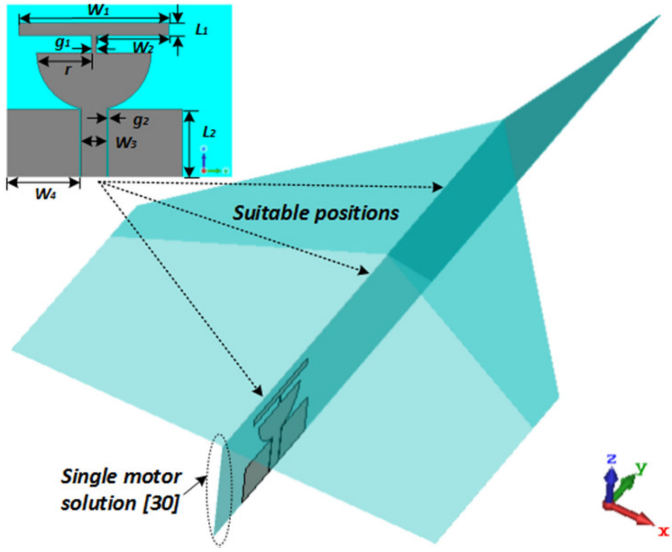

Fig. 13. Configuration of the realized optimized paper plane drone.

TABLE IV
Optimizes Antenna Dimension [mm]

L_1	L_2	W_1	W_2	W_3	W_4	g_1	g_2	r
2.5	13	30	14	5.2	14	1	0.2	11

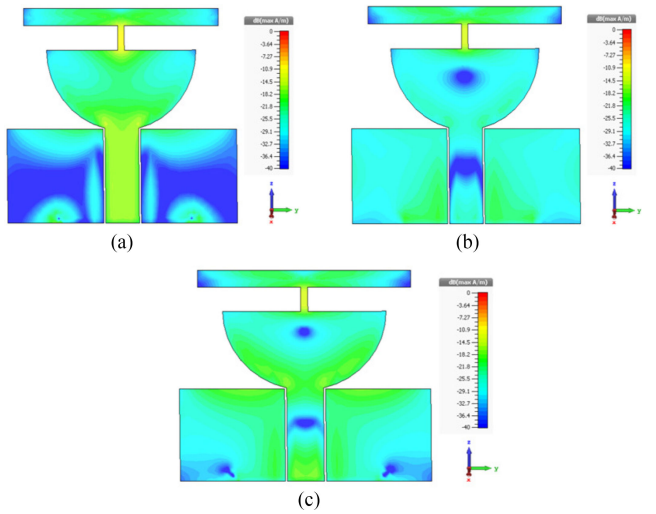

Fig. 14. Surface currents for the antenna design in Fig. 13. (a) 2.4 GHz. (b) 5.2 GHz. (c) 5.8 GHz.

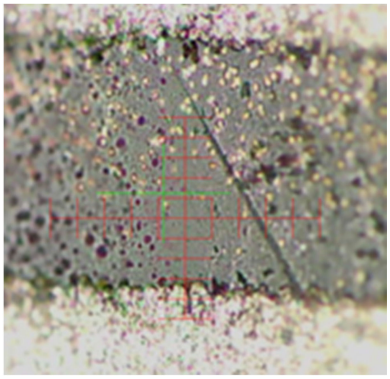

Fig. 15. Photograph of the printed metallic layers in the CPW transmission line.

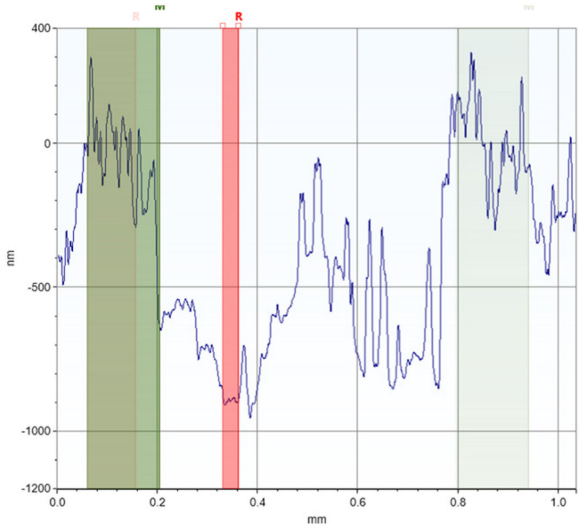

Fig. 16. Surface profile in the CPW transmission line.

B. Fabrication and Measurements

The antenna was realized using the same fabrication procedure described in Section II-B. A study of the printed layers and, in particular, in the gaps of the transmission line should provide a further insight of the fabrication process and its potential limitations. Fig. 15 shows a photograph of the conductive layers in a sample taken of the CPW transmission line of the antenna. As can be seen, there are many traces of silver ink in the channel and the edges of the tracks are non-uniform. A surface profile measured using the Veeco Dektak Stylus Profiler is shown in Fig. 16. The green area is the top of the silver surface, the red area is the bottom of the channel. The measured height difference is 825.69 nm. The additional texture to the right is likely to be caused by variation in the substrate surface and the stray silver particles.

Fig. 17 shows photographs of the printed antenna on the planar substrate and the folded origami drone. The folding lines are included. The antenna position on the paper substrate was calculated considering the sections where the drone needed to be folded. The same origami airplane and folding method as for the

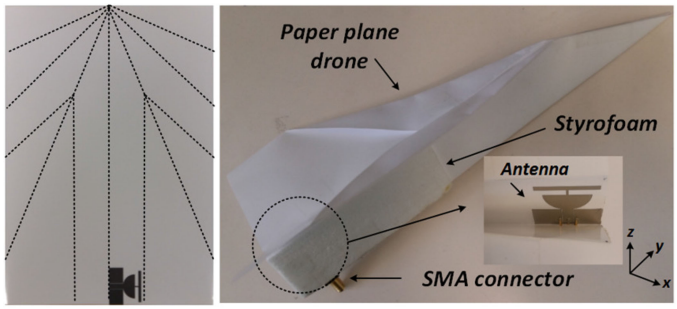

Fig. 17. Photograph of (a) printed planar photo sheet and (b) the folded origami paper plane drone and inside view.

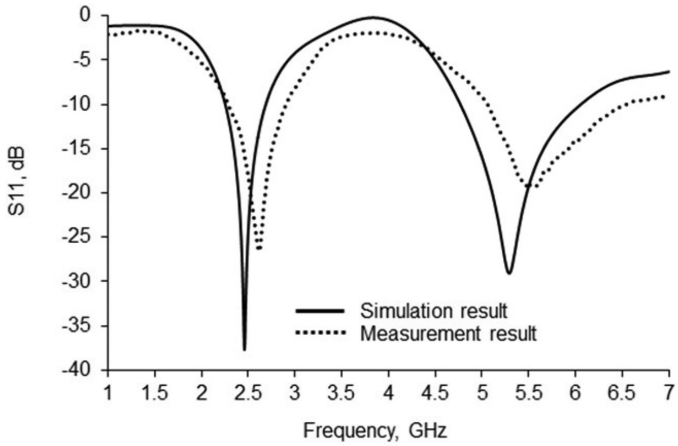

Fig. 18. Reflection coefficient (S_{11}) of the antenna for the optimized origami paper plane drone.

previous design were used. The antenna was designed so that it fits between the fold lines, thus avoiding potential cracks in the conductive layers. A 50 ohm SMA connector was attached to the bottom of the body of the drone. Styrofoam blocks ($\varepsilon_r \approx 1$) were placed on the left and right sides of the drone to hold the drone in shape during the measurements.

A basic thermal stability test on the antenna was carried out for the maximum and minimum temperature intended for operation. The structure was exposed to temperatures of -20 °C and 50 °C for 12 hours in separate experiments. In both cases, the effect on S_{11} was insignificant and the 2.4 GHz and 5 GHz bands were fully covered. Another potential mechanical stability test in aerospace is through vibration tests [34]. As the antenna is fully attached to the origami drone structure, it is expected to perform well in equivalent tests for this disposable drone application. The only concerning issue is likely to be wing deformation in the first antenna design, which was discussed in Section II-C.

The simulated and measured S_{11} are shown in Fig. 18. The measured resonant frequencies shifted slightly to the right. The measured first mode resonates at about 2.61 GHz with -10 dB impedance bandwidth of from 2.3 GHz to 2.9 GHz. The second resonance can be found at approximately 5.57 GHz with -10 dB bandwidth of from 5.0 GHz to 6.5 GHz. The measured

TABLE V
COMPARISON BETWEEN THE PROPOSED ANTENNA AND OTHER PREVIOUS ANTENNAS

Ref.	Freq. (GHz)	Gain (dB)	Bandwidth (GHz)	Size (mm^3)
[35]	2.45 5.5	1.3 4.8	0.1 1	50 x 50x 1.75
[36]	2.4 5.2	1.3 5. 15	0.5 0.2	50 x 75 x 0.8
[37]	2.45 5.8	2.75 5. 54	0.08 0.67	37.45 x 13 x 1.6
This work	2.4 5.2 5.8	1.9 2.6 3.1	0.6 1.5	35.4 x 30.8 x 0.18

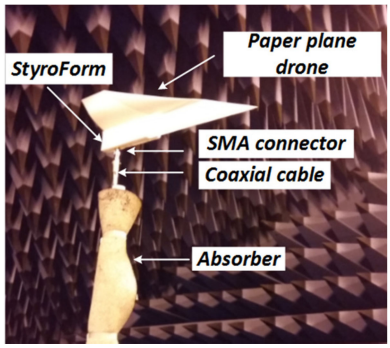

Fig. 19. Measurement setup for the origami paper drone antenna in anechoic chamber.

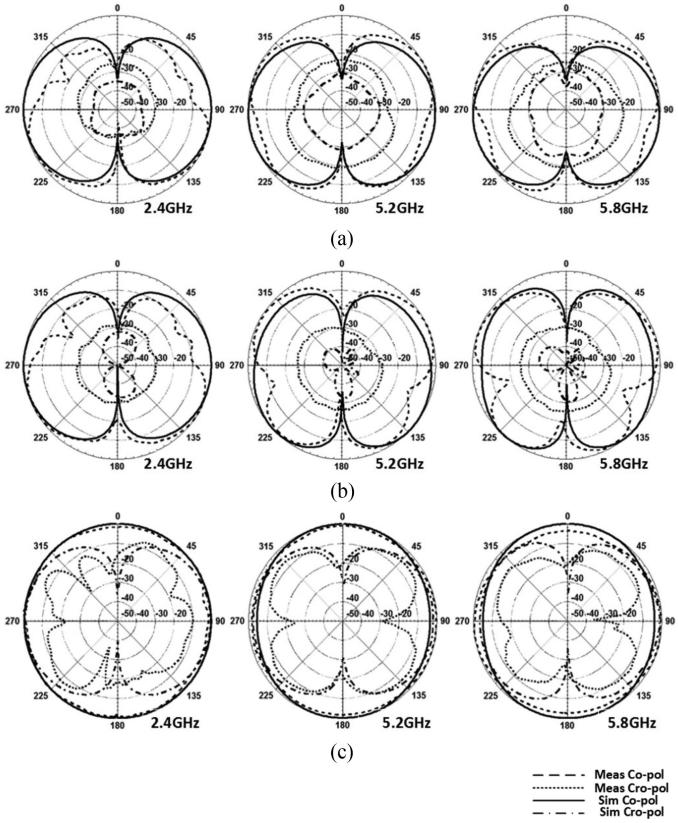

Fig. 20. Radiation patterns (a) at *xz* plane, (b) at *yz* plane, and (c) at *xy* plane.

S_{11} of the antenna covers the desired frequency of 2.4 GHz, 5.2 GHz and 5.8 GHz bands for the drone communication. The discrepancy between simulation and measurement is probably due to the fabrication issues discussed earlier as well as possible measurement errors. Table V gives the comparison of resonant frequency, gain, bandwidth, and size between the proposed antenna and the other previous antenna. The proposed antenna provides relatively wider bandwidth while keeping a small size at the corresponding frequency bands.

Fig. 19 shows the radiation pattern measurement set up. Fig. 20 shows a comparison between simulated and measured radiation patterns at 2.4 GHz, 5.2 GHz and 5.8 GHz respectively. The patterns in the *xz* plane are similar to the ones in *yz* plane with nulls along the *z*-axis. The patterns in the *xy* plane are mostly omnidirectional. The measured gains are 1.9 dB at 2.4 GHz, 2.6 dB at 5.2 GHz and 3.1 dB at 5.8 GHz. The measured gains are between 0.1 dB and 0.2 dB higher than the simulations due to the effect of connectors and coaxial cables. These differences can be clearly observed in the graphs.

IV. CONCLUSION AND DISCUSSION

Antennas suitable for integration with low cost inkjet printing electronics on disposable paper drones have been demonstrated. The best antenna solution for drone communication tends to be when the antenna is vertically polarized and omnidirectional. Different antenna positions are possible when considering paper drones. One possible scenario is when the electronics are located on the wings. In this case, an antenna can be located facing downwards and using the wings as a ground plane. A second case is when the electronics are in the lower section of the plane, in which case a CPW fed antenna can be hidden inside the plane. A CPW fed antenna can also be considered a more general solution as it can be rotated as required by the other electrical components of the drone.

A commercial desktop inkjet printer replaced with silver nanoparticle conductive ink cartridges can be used for the antenna fabrication. It has been proven to be an inexpensive and fast method with sufficient printed quality for this application.

The fabricated antennas have acceptable performance for efficient communication between the plane and a remote controller.

As a low-cost fabrication procedure, inkjet printing with off the shelf printers, with cartridges containing silver ink, may produce tracks with discontinuity at the edges and also unwanted deposition of inks across any channel. However, these fabrication errors do not seem to significantly affect the performance of the antennas at the frequency of operation of commercial drones.

In the future, disposable origami drones may include other electronic components which are also inkjet printed along the

antenna. This will create a fully integrated disposable drone solution. There is enough evidence from ongoing work by various research groups [25]–[27], and [30], [31] to support this vision. This paper has now contributed to this new field from the antenna perspective.

REFERENCES

[1] J. Berni, P. Zarco-Tejada, L. Suarez, and E. Fereres, "Thermal and narrowband multispectral remote sensing for vegetation monitoring from an unmanned aerial vehicle," *IEEE Trans. Geosci. Remote Sens.*, vol. 47, no. 3, pp. 722–738, Mar. 2009.

[2] Y. Nijsure, G. Kaddoum, N. Khaddaj Mallat, G. Gagnon, and F. Gagnon, "Cognitive chaotic UWB-MIMO detect-avoid radar for autonomous UAV navigation," *IEEE Trans. Intell. Transp. Syst.*, vol. 17, no. 11, pp. 3121–3131, Nov. 2016.

[3] H. Menouar, I. Guvenc, K. Akkaya, A. Uluagac, A. Kadri, and A. Tuncer, "UAV-Enabled intelligent transportation systems for the smart city: Applications and challenges," *IEEE Commun. Mag.*, vol. 55, no. 3, pp. 22–28, Mar. 2017.

[4] M. A. Goodrich *et al.*, "Supporting wilderness search and rescue using a camera-equipped mini UAV," *J. Field Robot.*, vol. 25, no. 1, pp. 89–110, Jan./Feb. 2008.

[5] H. Zhou, H. Kong, L. Wei, D. Creighton, and S. Nahavandi, "Efficient road detection and tracking for unmanned aerial vehicle," *IEEE Trans. Intell. Transp. Syst.*, vol. 16, no. 1, pp. 297–309, Feb. 2015.

[6] G. Cai, B. Chen, K. Peng, M. Dong, and T. Lee, "Modeling and control of the yaw channel of a UAV helicopter," *IEEE Trans. Ind. Electron.*, vol. 55, no. 9, pp. 3426–3434, Sep. 2008.

[7] L. Gupta, R. Jain, and G. Vaszkun, "Survey of important issues in UAV communication networks," *IEEE Commun. Surveys Tuts.*, vol. 18, no. 2, pp. 1123–1152, Apr./May 2016.

[8] S. Hayat, E. Yanmaz, and R. Muzaffar, "Survey on unmanned aerial vehicle networks for civil applications: A communications viewpoint," *IEEE Commun. Surveys Tuts.*, vol. 18, no. 4, pp. 2624–2661, Oct.–Dec. 2016.

[9] G. Virone *et al*., "Antenna pattern verification system based on a micro unmanned aerial vehicle (UAV)," *IEEE Antennas Wireless Propag. Lett.*, vol. 13, pp. 169–172, 2014.

[10] F. Namin, J. Petko, and D. Werner, "Analysis and design optimization of robust aperiodic micro-UAV swarm-based antenna arrays," *IEEE Trans. Antennas Propag.*, vol. 60, no. 5, pp. 2295–2308, May 2012.

[11] N. Neveu *et al.*, "Miniature hexaferrite axial-mode helical antenna for unmanned aerial vehicle applications," *IEEE Trans. Magn.*, vol. 49, no. 7, pp. 4265–4268, Jul. 2013.

[12] A. Barka, "Integration of antennas onboard vehicles and diffraction by large and complex structures with multiple-domain–multiple-methods techniques," *Proc. IEEE*, vol. 101, no. 2, pp. 280–297, Jan. 2013.

[13] Q. Liu *et al.*, "A novel broad beamwidth conformal antenna on unmanned aerial vehicle," *IEEE Antennas Wireless Propag. Lett.*, vol. 11, pp. 196–199, 2012.

[14] B.-H. Sun, Y.-F. Wei, S.-G. Zhou, and Q.-Z. Liu, "Low-profile and horizontally-polarised antenna for UAV applications," *Electron. Lett.*, vol. 45, no. 22, pp. 1106–1107, Oct. 2009.

[15] D. Kang, J. Tak, and J. Choi, "Wideband low-profile planar square segmented loop antenna for UAV applications," *Electron. Lett.*, vol. 52, no. 22, pp. 1828–1830, 2016.

[16] L. Scorrano, A. Di Rosa, B. Orobello, A. Manna, and F. Trotta, "Experimental investigations of a novel lightweight blade antenna for UAV applications [antenna applications corner]," *IEEE Antennas Propag. Mag.*, vol. 59, no. 2, pp. 108–178, Apr. 2017.

[17] J. Chen, K.-F. Tong, and J. Wang, "A triple band arc-shaped slot patch antenna for UAV GPS/Wi-Fi applications," in *Proc. Int. Symp. Antennas Propag.*, 2013, vol. 1, pp. 367–370.

[18] G. D. Goh, S. Agarwala, G. L. Goh, V. Dikshit, S. L. Sing, and W. Y. Yeong, "Additive manufacturing in unmanned aerial vehicles (UAVs): Challenges and potential," *Aerosp. Sci. Technol.*, vol. 63, pp. 140–151, 2017.

[19] A. Rida, L. Yang, T. Reynolds, E. Tan, S. Nikolaou, and M. M. Tentzeris, "Inkjet-printing UHF antenna for RFID and sensing applications on liquid crystal polymer," in *Proc. IEEE Antennas Propag. Soc. Int. Symp.*, Jun. 2009, pp. 1–4.

[20] B. K. Tehrani, B. S. Cook, and M. M. Tentzeris, "Inkjet printing of multilayer millimeter-wave Yagi-Uda antennas on flexible substrates," *IEEE Antennas Wireless Propag. Lett.*, vol. 15, pp. 143–146, 2016.

[21] B. Cook, B. Tehrani, J. Cooper, and M. Tentzeris, "Multilayer inkjet printing of millimeter-wave proximity-fed patch arrays on flexible substrates," *IEEE Antennas Wireless Propag. Lett.*, vol. 12, pp. 1351–1354, 2013.

[22] H. R. Khaleel, "Design and fabrication of compact inkjet printed antennas for integration within flexible and wearable electronics," *IEEE Trans. Compon. Packag. Technol.*, vol. 4, no. 10, pp. 1722–1728, Oct. 2014.

[23] H. F. Abutarboush and A. Shamim, "Paper-Based inkjet-printed tri-band U-Slot monopole antenna for wireless applications," *IEEE Antennas Wireless Propag. Lett.*, vol. 11, pp. 1234–1237, 2012.

[24] M. Nikfalazar *et al.*, "Steerable dielectric resonator phased-array antenna based on inkjet-printed tunable phase shifter with BST metal-insulator-metal varactors," *IEEE Antennas Wireless Propag. Lett.*, vol. 15, pp. 877–880, 2016.

[25] P. Pounds, "Paper plane: Towards disposable low-cost folded cellulose-substrate UAVs," in *Proc. Australasian Conf. Robot. Autom.*, 2012, pp. 144–152.

[26] Evan Ackerman, "Swarms of disposable drones will make critical deliveries and then Vanish," IEEE Spectrum. Web. Feb. 2017. [Online]: Available:http://spectrum.ieee.org/automaton/robotics/drones/otherlab-apsara-aerial-delivery-system. Accessed in Aug. 2017.

[27] G. Grau, E. J. Frazier, and V. Subramanian, "Printed unmanned aerial vehicles using paper-based electroactive polymer actuators and organic ion gel transistors," *Microsyst. Nanoeng.*, vol. 2, 2016, Art. no. 16032.

[28] J. Romeu, A. Aguasca, J. Alonso, S. Blanch, and R. R. Martins, "Small UAV radiocommunication channel characterization," in *Proc. 4th Eur. Conf. Antennas, Propag.*, Apr. 2010, pp. 1–5.

[29] CST Microwave Studio. [Online] http://www.cst.com. Accessed in: Dec. 2017.

[30] PowerUp. [Online]: Available: https://www.poweruptoys.com/Accessed in: Aug. 2017.

[31] P. Pounds and S. Singh, "Integrated electro-aeromechanical structures for low-cost, self-deploying environment sensors and disposable UAVs," in *Proc. IEEE/RAS Int. Conf. Robot. Autom.*, 2013, pp. 4459–4466.

[32] S. Nikolaou and M. A. B. Abbasi, "Design and development of a compact UWB monopole antenna with easily-controllable return loss," *IEEE Trans. Antennas Propag.*, vol. 65, no. 4, pp. 2063–2067, Apr. 2017.

[33] AgIC Inc., [online]: Available: https://agic.cc/en/ Accessed in: Dec. 2017.

[34] N. F. Chamberlain, R. E. Hodges, and M. S. Zawadzki, "Metal patch antenna," United States Patent 8,169,371, May 2012.

[35] Y. Lu and Y. Lin, "A mode based design method for dual-band and self-diplexing antennas using double T-stubs loaded aperture," *IEEE Trans. Antennas Propag.*, vol. 60, no. 12, pp. 5596–5603, Dec. 2012.

[36] Y.-L. Kuo and K.-L. Wong, "Printed double-T monopole antenna for 2.4/5.2 GHz dual-band WLAN operations," *IEEE Trans. Antennas Propag.*, vol. 51, no. 9, pp. 2187–2192, Sep. 2003.

[37] I.-F. Chen and C.-M. Peng, "Microstrip-fed dual-U-shaped printed monopole antenna for dual-band wireless communication applications," *Electron Lett.*, vol. 39, pp. 955–956, 2003.

Authors' photographs and biographies not available at the time of publication.